Wave-front generation of Zernike polynomial modes with a micromachined membrane deformable mirror

Lijun Zhu, Pang-Chen Sun, Dirk-Uwe Bartsch, William R. Freeman, and Yeshaiahu Fainman

We investigate the characteristics of a 37-channel micromachined membrane deformable mirror for wave-front generation. We demonstrate wave-front generation of the first 20 Zernike polynomial modes, using an iterative algorithm to adjust driving voltages. The results show that lower-order-mode wave fronts can be generated with good accuracy and large dynamic range, whereas the generation of higher-order modes is limited by the number of the actuator channels and the working range of the deformable mirror. The speed of wave-front generation can be as fast as several hundred hertz. Our results indicate that, in addition to generation of wave fronts with known aberrations, the characteristics of the micromachined membrane deformable mirror device can be useful in adaptive optics systems for compensating the first five orders of aberration. © 1999 Optical Society of America

OCIS codes: 101.1080, 220.1000, 230.6120, 230.4040.

1. Introduction

Zernike polynomials have been widely used in astronomy for decades to describe wave-front aberrations that are due to atmospheric turbulence.[1,2] Recently they have also been actively used in vision sciences to describe wave-front aberrations of the human eye.[3,4] Zernike polynomials are a complete and orthogonal polynomial set defined on the unit circle. Wave-front aberrations over a circular optical aperture can be conveniently described with Zernike polynomials; and some classical aberrations such as spherical aberration, astigmatism, coma, and the like, are related to certain Zernike polynomial modes.[5] Synthesis of wave fronts corresponding to Zernike polynomial modes will be useful for simulating wave-front aberrations that are due to atmospheric turbulence or for simulating aberrations of the eye. The synthesized wave fronts can be used to test the adaptive optics systems designed to compensate for wave-front aberrations. The capability of a device for generating Zernike-mode wave fronts also indicates its capability for compensating for the corresponding aberrations. Liquid-crystal spatial light modulators have been investigated for wave-front generation or correction.[6–8] However, they have limited modulation ranges, slow time responses, and currently require operations with polarized light. Binary computer-generated holograms based on ferroelectric liquid-crystal spatial light modulators are also demonstrated to generate wave fronts with higher speed but with the penalty of reduced optical throughput.[9] Although conventional deformable mirrors used in adaptive astronomical imaging systems would be suitable for wave-front generation, they are usually big and expensive, making them impractical for low-cost applications.

In this paper we demonstrate the use of a compact low-cost multichannel micromachined membrane deformable mirror (MMDM) to generate Zernike-mode wave fronts. MMDM devices have recently been developed for operations at moderate speeds (e.g., a few hundred hertz).[10] They have the potential to be used as low-cost corrective elements in adaptive optics systems for various practical applications such as correcting aberrations of human eyes and as laser beams. However, the characteristics of the MMDM for wave-front generation or aberration compensa-

L. Zhu (lzhu@ucsd.edu), P.-C. Sun, and Y. Fainman are with the Department of Electrical and Computer Engineering, University of California San Diego, La Jolla, California 92093. D.-U. Bartsch and W. R. Freeman are with the UCSD Shiley Eye Center, Department of Ophthalmology, University of California San Diego, La Jolla, California 92093.

Received 9 June 1999; revised manuscript received 8 July 1999.
0003-6935/99/286019-08$15.00/0

tion have not been well investigated, owing to the difficulty in controlling this device. Because of the nonlinear and coupled responses of control channels, it is not straightforward to obtain the required driving voltages for desired mirror surface shapes. We developed an iterative control algorithm based on experimentally measured MMDM response characteristics and were able to use a 19-channel MMDM to compensate for some aberrations of a model eye in an adaptive optics system.[11] However, this previous algorithm was developed only for aberration compensation with the desired reflected wave front being a plane wave. In this paper we show how we modify the adaptive algorithm to generate arbitrary reflected wave fronts such as wave fronts of individual Zernike modes or of any combination of Zernike modes. We demonstrate the production of the first 20 Zernike modes with a dynamic range of several wavelengths, using a 37-channel MMDM. A Hartmann–Shack wave-front sensor (HSWS) and a null interferometer are used to qualitatively and visually measure the generated wave fronts. The results show that lower-order modes can be generated with good accuracy and large dynamic range, whereas the generation of higher-order modes is limited by the working range and the channel number of the MMDM device. The ability to generate Zernike-mode wave fronts is useful for characterization of the MMDM for compensating aberrations described by Zernike modes.

2. Experimental System

We use a 37-channel MMDM device (OKO Technologies, The Netherlands) to generate Zernike-mode wave fronts. The MMDM device consists of an aluminum-coated silicon nitride membrane with 37 electrostatic electrodes underneath. The electrostatic forces between the membrane and the electrodes pull down the membrane and modulate the shape of the membrane. The device has a circular aperture of 15 mm in diameter with its boundary attached to the supporting substrate. The center of the membrane can be deformed to as much as 7 μm. We use the central 12-mm-diameter circular part of the membrane as an active aperture of the device, thereby allowing for modulation of the wave fronts at the edge of the active aperture (Fig. 1). Since the membrane can be deformed only in the direction toward the control electrodes, an initial bias is necessary. This bias is achieved by use of a divergent incident spherical wave front. More detailed descriptions of the MMDM device can be found in Refs. 10 and 11.

The experimental optical system setup with the MMDM is shown in Fig. 2. A laser beam is expanded by a spatial filter and collimated by lens L0. The expanded laser beam is projected onto the MMDM by lenses L1 and L2. Since the MMDM surface can be deformed only into a concave shape, L2 is displaced slightly to provide a divergent spherical wave-front bias in the MMDM plane. The MMDM is tilted to separate the incident and the reflected

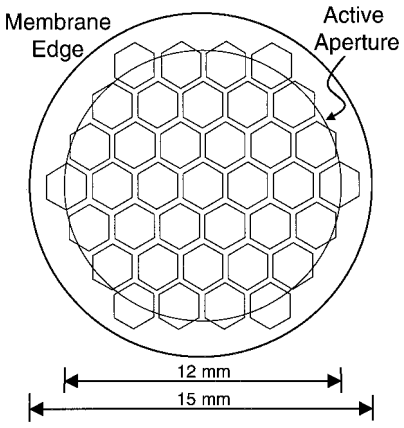

Fig. 1. Electrode layout of the 37-channel MMDM.

beams by an angle of 20 deg. Although the tilt of the MMDM introduces some aberrations, these aberrations along with initial aberrations that are due to imperfection of the MMDM surface can be corrected by setting of the mirror shapes. The tilt improves the light efficiency without use of a beam splitter to separate the incident and the reflected beams and shows the flexibility of using the MMDM. The reflected wave front is next imaged onto the HSWS measurement plane with L3, L4, and BS2. The wave front is analyzed and fitted to the Zernike polynomial wave-front description. To evaluate the synthesized wave fronts visually in real time, we also introduce an interferometric measurement. A CCD camera is used to detect the interference between the synthesized wave front (image of the reflected wave front by the MMDM) and a reference plane wave obtained from the original collimated laser beam with BS1, a flat mirror, and the reflection through the BS2 (see dotted path in Fig. 2). The optical paths of the

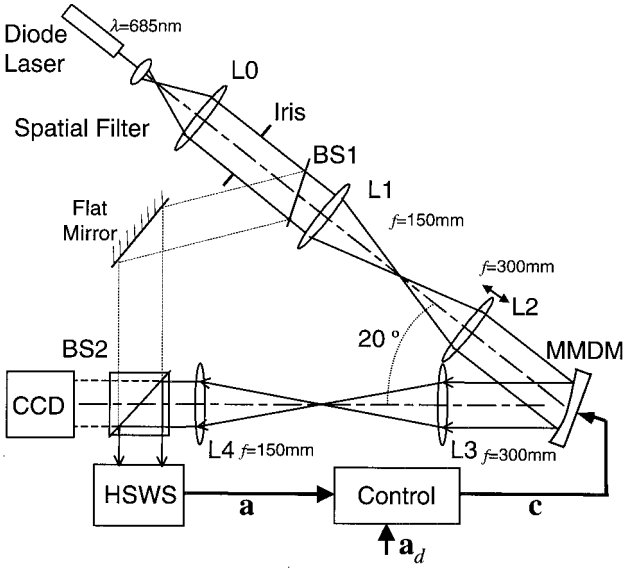

Fig. 2. Experimental adaptive optical system used to generate wave fronts of Zernike polynomial modes with the MMDM.

synthesized wave front and the reference wave front have approximately the same length, providing good contrast of interference pattern. The flat mirror is carefully adjusted to obtain the null interferogram. The reference beam is blocked when HSWS wave-front measurements are performed. The HSWS consists of a lenslet array and a CCD camera located in the focal plane of the lenslet. The wave front is reconstructed from the measured slopes of the wave front at subapertures of the lenslet array detected from the HSWS image.[11] The measured wave front is then fed into our control algorithm described below to drive the MMDM actuators in a closed-loop configuration. This procedure is performed iteratively until the desired wave front is synthesized. A Pentium II personal computer running our software in Matlab and C++ is used to implement the algorithm in the closed-loop iterative system.

3. Algorithm for Producing Zernike-Mode Wave Fronts

In the past we developed an adaptive control algorithm to achieve optimum MMDM surface shapes to compensate for aberrations of a model eye producing a plane wave reflected from the MMDM device. The principle of our adaptive algorithm is based on the measurement of the wave-front error between the desired wave front $\varphi_d(x, y)$ and the actual wave front $\varphi(x, y)$ that is reflected from the MMDM and measured with the HSWS. The algorithm calculates a small adjustment of driving voltages that will reduce the wave-front error and make the wave front $\varphi(x, y)$ gradually converge to the desired wave front $\varphi_d(x, y)$. For our previous application for eye aberration compensation we used a plane wave as the desired wave front $\varphi_d(x, y)$. In contrast in this manuscript we show that the wave front $\varphi_d(x, y)$ can be any arbitrary wave fronts such as the wave fronts of single Zernike modes or of any combination of Zernike modes.

The wave front $\varphi(x, y)$ is expressed in terms of Zernike polynomial decomposition, described by

$$\phi(x, y) = \sum_{k=1}^{M} a_k z_k(x, y) + \delta\phi(x, y) \tag{1}$$

where $\varphi(x, y)$ is defined as the actual wave fronts as a function of spatial coordinates x and y within the beam aperture; M is the total number of Zernike polynomials used, $z_k(x, y)$ is the kth Zernike polynomial with a_k being its coefficient, and $\delta\varphi(x, y)$ is the error due to the truncation of using only M Zernike polynomials. A set of Zernike coefficients $\{a_1, a_2, \ldots, a_M\}$ or a vector $\mathbf{a} = [a_1, a_2, \ldots, a_M]^T$, can be used to describe the wave front $\varphi(x, y)$, where superscript T stands for matrix transpose. The wave front $\varphi(x, y)$ reflected from the MMDM is measured with the HSWS (see Fig. 2). A modal wave-front reconstruction algorithm with the basis of Zernike polynomials is used to calculate Zernike coefficients of the wave front $\varphi(x, y)$.[11]

The error between $\varphi(x, y)$ and $\varphi_d(x, y)$ can be described with the wave-front variance σ^2 over the entire aperture of the beam,

$$\sigma^2 = \frac{1}{A} \iint_{\text{aperture}} [\phi(x, y) - \phi_d(x, y)]^2 dx dy, \tag{2}$$

where A is the area of the beam aperture. This error can be calculated with Zernike coefficients by

$$\begin{aligned} \sigma^2 &= \sum_{k=1}^{M} (a_k - a_{dk})^2 w_k^2 + \delta\sigma^2 \\ &= \|(\mathbf{a} - \mathbf{a}_d) * \mathbf{w}\|^2 + \delta\sigma^2, \end{aligned} \tag{3}$$

with w_k^2 defined by

$$w_k^2 = \frac{1}{A} \iint_{\text{aperture}} [z_k(x, y)]^2 dx dy, \tag{4}$$

where $\mathbf{a}_d = [a_{d1}, a_{d2}, \ldots, a_{dM}]^T$ represents the desired wave front; $\mathbf{w} = [w_1, w_2, \ldots, w_M]$ is a vector determined from Zernike polynomials with Eq. (4), and the $*$ operator denotes the element-by-element multiplication of two vectors. Note that the beam aperture is normalized with the beam radius to the unit circle to keep the orthogonality of Zernike polynomials so that the integration of the cross terms of Zernike polynomials over the unit circle is zero.

In our system shown in Fig. 2 the wave front reflected from the MMDM, represented by vector $\mathbf{a}$, is measured with the HSWS. Following a deduction similar to that described in Ref. 11, we obtain a recursive equation to iteratively adjust driving voltages to reduce σ^2 to its minimum, yielding

$$\mathbf{c}_{\text{new}} = \mathbf{c}_{\text{old}} - 2\mu\mathbf{B}^T[(\mathbf{a} - \mathbf{a}_d) * \mathbf{w}^2], \tag{5}$$

where vector $\mathbf{c} = [V_1^2, V_2^2, \ldots, V_P^2]^T$ represents driving voltages V_l ($l = 1, 2, \infty, \text{P}$) applied to the electrodes of the MMDM with total number of electrodes (channels) as P; $\mathbf{B}$ is an $M \times P$ matrix representing the response characteristics of the MMDM and can be measured experimentally[11]; μ is a positive scalar representing the convergence rate, and its value is determined empirically; and $\mathbf{w}^2 = [w_1^2, w_2^2, \ldots, w_M^2]$ is calculated with Eq. (4). In practice $\mathbf{w}^2$ can be regarded as weighting factors of Zernike coefficients to optimize the convergence rate of each coefficient. By iteratively adjusting the vector $\mathbf{c}$ of the driving voltages with Eq. (5), the wave front $\varphi(x, y)$ will converge to the desired wave front $\varphi_d(x, y)$ with a minimum value of σ^2. To generate the wave front of a single Zernike mode with the desired quantity, we set the corresponding element of $\mathbf{a}_d$ to the desired value while setting all other elements to zero. When we start with an arbitrary set of initial driving voltages and iteratively update the driving voltages with Eq. (5), the output wave front will be altered toward the desired Zernike mode.

Table 1. Zernike Polynomials and Their Meaning[a,b]

Mode k	Order n	Norm. Factor N_k	Polynomial $z_k(\rho, \theta)$	Meaning
0	0	1	1	Piston
1	1	4	$\rho \sin \theta$	Tilt in x direction
2		4	$\rho \cos \theta$	Tilt in y direction
3	2	6	$\rho^2 \sin 2\theta$	Astigmatism ($\pm 45°$)
4		3	$2\rho^2 - 1$	Defocusing
5		6	$\rho^2 \cos 2\theta$	Astigmatism (0° and 90°)
6	3	8	$\rho^3 \sin 3\theta$	Triangular astigmatism
7		8	$(3\rho^3 - 2\rho)\sin \theta$	Coma
8		8	$(3\rho^3 - 2\rho)\cos \theta$	Coma
9		8	$\rho^3 \cos 3\theta$	Triangular astigmatism
10	4	10	$\rho^4 \sin 4\theta$	Spherical aberration
11		10	$(4\rho^4 - 3\rho^2)\sin 2\theta$	
12		5	$6\rho^4 - 6\rho^2 + 1$	
13		10	$(4\rho^4 - 3\rho^2)\cos 2\theta$	
14		10	$\rho^4 \cos 4\theta$	
15	5	12	$\rho^5 \sin 5\theta$	
16		12	$(5\rho^5 - 4\rho^3)\sin 3\theta$	
17		12	$(10\rho^5 - 12\rho^3 + 3\rho)\sin \theta$	
18		12	$(10\rho^5 - 12\rho^3 + 3\rho)\cos \theta$	
19		12	$(5\rho^5 - 4\rho^3)\cos 3\theta$	
20		12	$\rho^5 \cos 5\theta$	

[a] θ is defined as the angle with y axis.
[b] Ref. 5.

4. Production of Zernike-Mode Wave Fronts

Employing the above adaptive optics algorithm, we generate wave fronts of the first 20 Zernike polynomial modes ($M = 20$), which cover the first five orders of Zernike polynomials. The definition of Zernike polynomials in Ref. 5 is used with their analytical forms in the polar coordinate system listed in Table 1, where the order number and the normalization factor are also included. The normalization factors N_k satisfy the equation

$$w_k^2 = 1/N_k, \tag{6}$$

and the wave-front variance between the generated wave front $\varphi(x, y)$ and the desired $\varphi_d(x, y)$ can be calculated by use of their Zernike coefficients by

$$\sigma^2 = \left[\sum_{k=1}^{M} \frac{(a_k - a_{dk})^2}{N_k}\right] + \delta\sigma^2, \tag{7}$$

where $\delta\sigma^2$ is the error owing to the truncation to the finite number of Zernike polynomials. The error $\delta\sigma^2$ is ignored in our calculation as discussed later in this section. Some of the Zernike modes are related to classical aberrations (see Table 1); for example, the 4th mode is the defocus, the 3rd and the 5th terms are related to astigmatism, the 7th and the 8th terms are related to coma, and the 12th term describes spherical aberration. Within the same order, sine and cosine modes have symmetric analytical forms. They have the same wave-front shapes but with a rotational angle with respect to each other. For example, modes 1 and 2 are tilts along x and y directions, respectively; modes 3 and 5 are astigmatisms about the $\theta = 45°$axis and the $\theta = 0°$ axis, respectively.

In our experiments the beam aperture and the wave front are normalized with the beam radius of $r = 3$ mm measured in the plane of the HSWS. We obtain elements of matrix $\mathbf{B}$ experimentally by measuring MMDM responses to all electrodes as described in Ref. 11. In the closed-loop system shown in Fig. 2, driving voltages are updated with Eq. (5) in each step. If the calculated voltages are out of the permitted voltage range, the voltages are set to the extreme voltages (0 or 200 V). The vector $\mathbf{w}^2$ is simply set to a unit vector, whereas μ is determined experimentally with a compromise of the convergence speed and residual errors. After convergence we do not observe significant oscillations.

To produce the wave front of each Zernike mode, we set the desired value of the corresponding element of $\mathbf{a}_d$ to various values from -4×10^{-4} to 4×10^{-4} with a step increment of 1×10^{-4} and all other elements of $\mathbf{a}_d$ to zeros. Each wave front is produced with 20 iterations. Figures 3(a) and 3(b) show results of Zernike coefficients of the generated wave fronts of first 20 modes obtained by setting of the corresponding coefficients to 3×10^{-4} and -3×10^{-4}, respectively. In Table 2 we summarize the generated wave fronts shown in Fig. 3(a) by listing the corresponding values of the Zernike coefficients for the generated wave fronts. Root-mean-square (rms) variances of these wave fronts compared with the

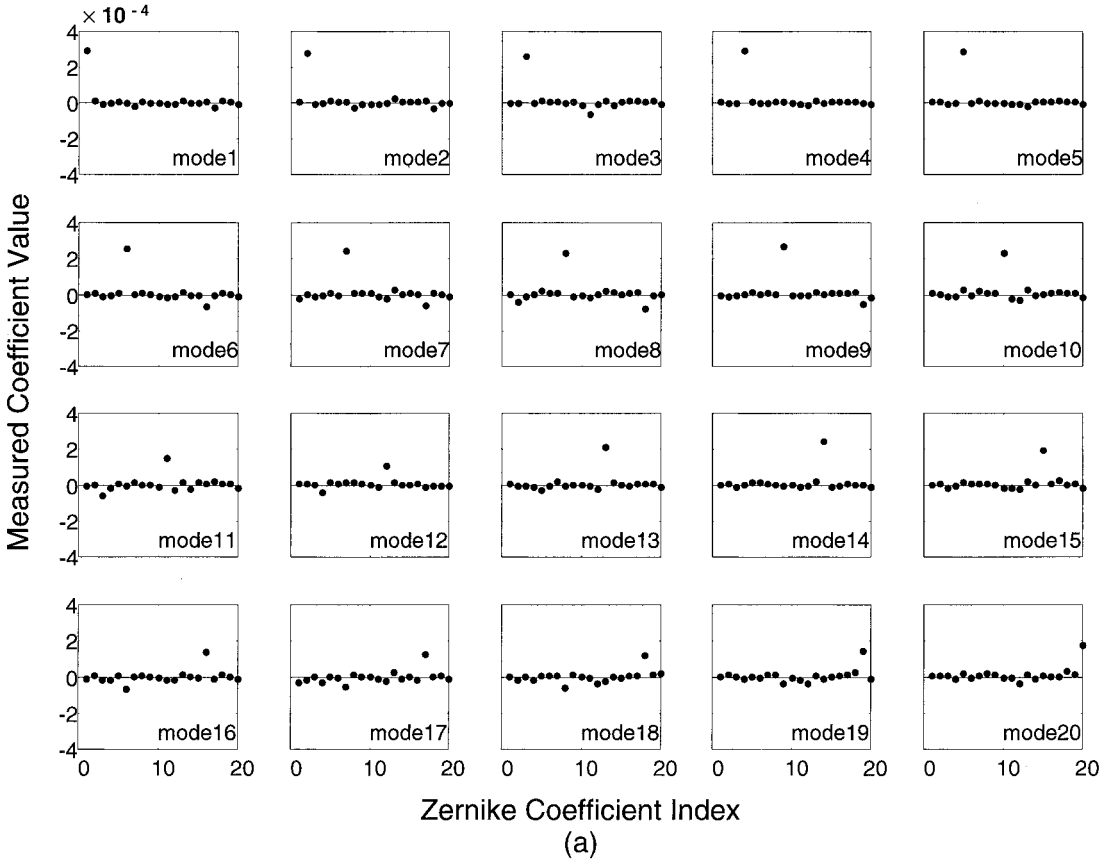

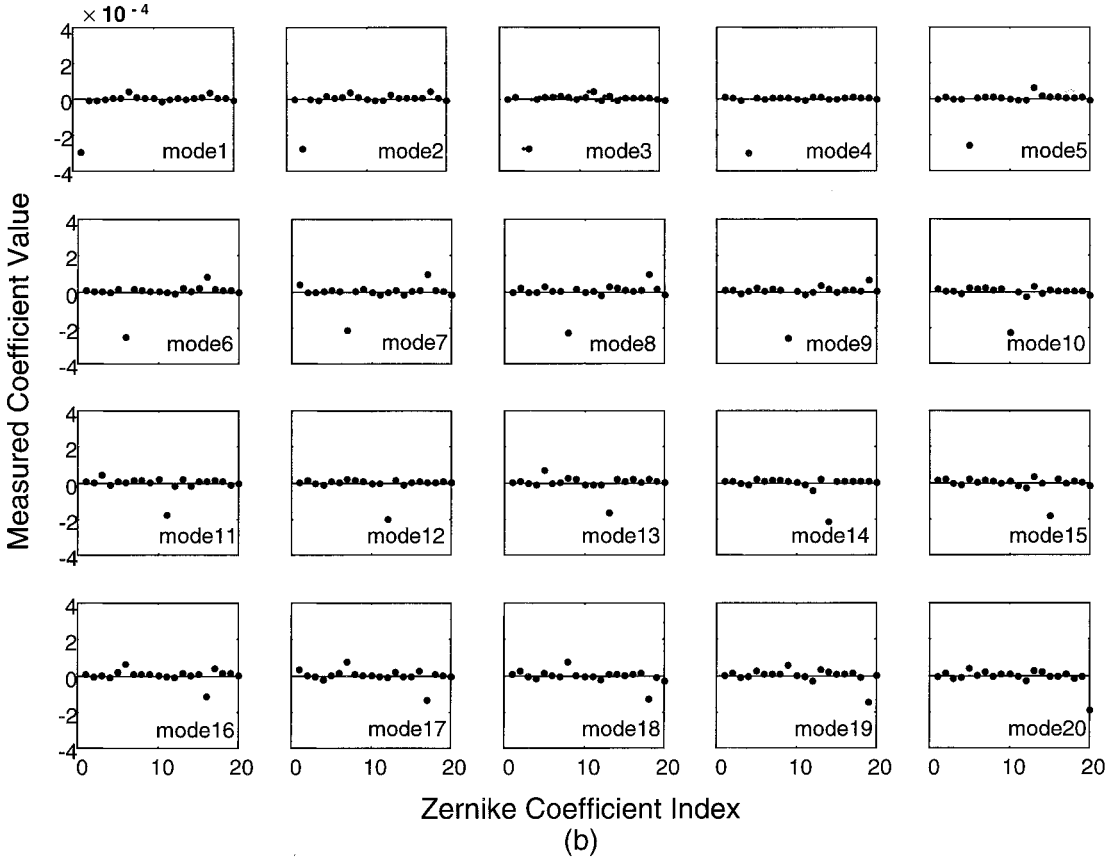

Fig. 3. Measured Zernike coefficients of wave fronts of the first 20 Zernike modes generated in the experimental system with target coefficients of (a) 3×10^{-4} and (b) -3×10^{-4}.

Table 2. Values of the Corresponding Zernike Coefficients of Generated Wave-Front Modes and their rms Wave-Front Variances from the Ideal Wave Fronts with the Same Zernike Coefficient Values

	Mode Index k									
	1	2	3	4	5	6	7	8	9	10
a_k ($\times 10^{-4}$)	2.96	2.82	2.64	2.96	2.87	2.60	2.47	2.31	2.67	2.30
rms variance (λ)	0.08	0.08	0.10	0.04	0.05	0.10	0.11	0.15	0.09	0.11
	Mode Index k									
	11	12	13	14	15	16	17	18	19	20
a_k($\times 10^{-4}$)	1.53	1.10	2.14	2.47	1.97	1.41	1.28	1.23	1.45	1.74
rms variance (λ)	0.14	0.10	0.08	0.06	0.09	0.13	0.14	0.13	0.11	0.10

ideal wave fronts of individual Zernike modes with the same coefficients are also calculated and listed in Table 2, where the truncation error is ignored when we calculate the wave-front variance with Eq. (7). As shown in Fig. 3(a) and in Table 2, for each generated wave front within the 3rd-order (modes 1–9), the coefficients are close to the target value of 3×10^{-4} and all other coefficients are close to zero. However, high-order modes (modes 10–20) can be generated with somewhat limited maximum values of the corresponding coefficients, indicating that the MMDM is limited in generating a large dynamic range for high-order modes, owing to limited number of control channels. Nevertheless, the generated modes provide sufficient accuracy for many applications with rms variance from the corresponding ideal modes of

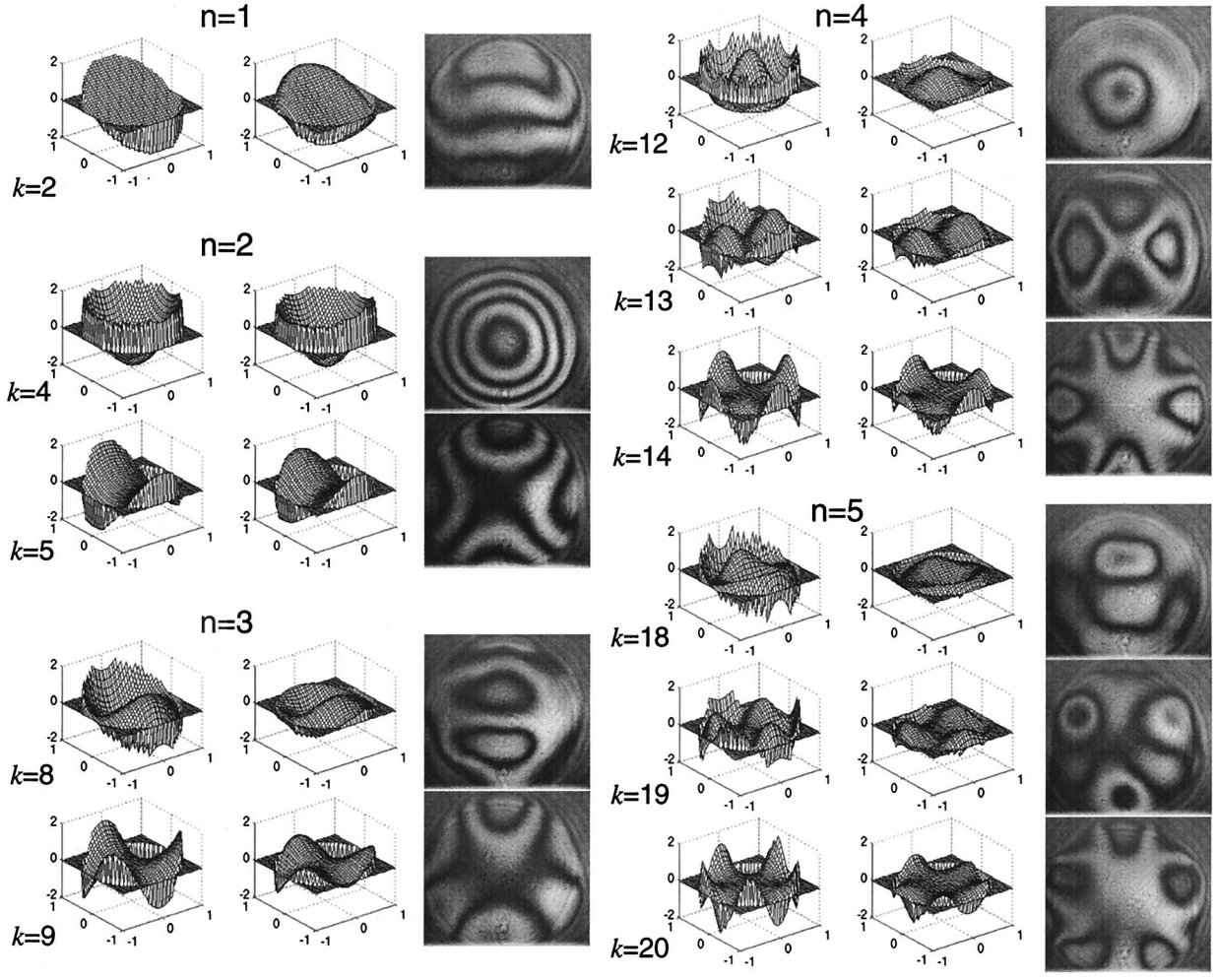

Fig. 4. Target wave fronts with coefficient of 4×10^{-4} (column 1), generated wave fronts (column 2), and null interferograms of the generated wave fronts interfered with a reference plane wave (column3). In wave-front plots of the first and second columns, the unit of the z axis is the number of wavelengths.

less than 0.15λ (wavelength λ = 0.685 μm is used in our experiments). Some modes are very accurately generated with the rms variance of less than 0.1λ. The generated desired modes are also accompanied by other undesired modes. For example, mode 17 is significant along with desired mode 7, and mode 18 appears in addition to desired mode 8 (see Fig. 3). The coupling between these modes occurs, because they have similar shapes (see sample wave-front shapes in Fig. 4 for $k = 8$ and $k = 18$) that are difficult to synthesize distinctly with a limited number of control channels. The results indicate that, with 37 actuator channels, the MMDM can be used to compensate for low-order (up to 3rd order) and for a certain amount of the high-order aberrations. Comparing Figs. 3(a) and 3(b), we find the asymmetry of the MMDM for wave-front generation of Zernike modes with positive and negative coefficients. The MMDM operates better in one direction than in the other, as is clearly seen from mode 12, which can be generated with larger amounts and better accuracy for negative target coefficients than for positive target coefficients. This asymmetry occurs because the membrane can be deformed only in one direction. It is also related to the applied incident spherical wave-front bias. By choosing a proper bias, we can easily eliminate the asymmetry of the defocus term, but the asymmetry of the high-order modes is difficult to eliminate simultaneously.

For real-time visualization of the generated Zernike-mode wave fronts we use an interferometric setup shown in Fig. 2. We use a null interferogram of the generated wave front interfered with a well-aligned and well-tested plane wave. Figure 4 shows the target wave fronts with a corresponding coefficient of 4×10^{-4} (first column), actual generated wave fronts under this target (second column), and the corresponding interferograms (third column) for the first five orders of Zernike polynomials. A coefficient of 4×10^{-4} of a Zernike-mode wave front corresponds a peak-to-valley value of 3.5λ within the beam aperture in our system with the normalization by the beam radius $r = 3$ mm and wavelength λ = 0.685 μm. Figure 4 shows only cosine modes in Table 1 of each order, because sine modes are similar to the corresponding cosine modes only with a difference of rotation angle. From Fig. 4 we can see again that generated wave fronts are close to the target wave fronts for lower modes with peak-to-valley values of ~3.5λ. For high-order modes the amplitude of generated wave fronts is smaller with peak-to-valley values of ~2λ.

In our experiment 20 Zernike polynomials are used to describe the wave fronts. The accuracy of the measured wave fronts is affected by the truncation of Zernike polynomials as described in Eq. (1). Therefore the calculated rms variances listed in Table 2 will be slightly smaller than actual rms variances. However, as shown in our results, since the capability of the MMDM for generating wave fronts of high-order Zernike polynomials is limited by the structure of the MMDM, the high-order components existing in the generated wave fronts will be relatively small. Therefore the truncation error is ignored in our calculation. Using additional Zernike polynomials can reduce the truncation error, but the accuracy improvement will be limited. In our system the measurement accuracy of the generated wave fronts is also verified by the null interferometer shown in Fig. 2. The obtained interferograms in Fig. 4 show a good accuracy of the generated wave fronts.

5. Conclusions

We have generated wave fronts of 20 Zernike modes, using a 37-channel MMDM with an iterative algorithm to adjust the driving voltages step by step to generate desired wave fronts. The results show that lower-order wave-front modes can be generated with high accuracy and large dynamic range and that high-order wave-front modes can be generated with smaller dynamic range. The number of control actuators and the working range of the membrane limit the capability of the MMDM to generate high-order wave-front modes. We have also measured the time response of the MMDM, showing that the speed can be as great as several hundred hertz.[12] Although we use 20 iterations to generate each Zernike wave-front mode, the voltages for each wave front can be stored in a lookup table so that the MMDM can be operated with its full speed for dynamic production of the wave fronts in the lookup table. Our results indicate that the MMDM can be used to generate wave fronts of the first five orders of Zernike polynomials with good accuracy and at sufficient speeds for most applications. In addition to generation of wave fronts with known aberrations for testing the adaptive optics systems, the characteristics of the MMDM show that this device can be useful for compensating aberrations up to the 5th order. Promising applications include adaptive optics systems for aberration compensation of the human eye and phase aberration compensation for high-quality laser beams, as well as systems that use high-quality dynamic focusing with aberration compensation.

This research was supported in part by a grant from the Whitaker Foundation and the National Science Foundation.

References

1. R. J. Noll, "Zernike polynomials and atmospheric turbulence," J. Opt. Soc. Am. **66,** 207–211 (1976).
2. J. Y. Wang and D. E. Silva, "Wave-front interpretation with Zernike polynomials," Appl. Opt. **19,** 1510–1518 (1980).
3. J. Liang and D. R. Williams, "Aberrations and retinal image quality of the normal human eye," J. Opt. Soc. Am. A **14,** 2873–2883 (1997).
4. L. N. Thibos, R. A. Applegate, H. C. Howland, D. R. Williams, P. Artal, R. Navarro, M. C. Campbell, J. E. Greivenkamp, J. T. Schwiegerling, S. A. Burns, D. A. Atchison, G. Smith, and E. J. Sarver, "A VSIA sponsored effort to develop methods and standards for the comparison of the wavefront aberration structure of the eye between devices and laboratories," in Digest of Topical Meeting on Vision Science and Its Applications (Optical Society of America, Washington D.C., 1999), pp. 236–239.
5. D. Malacara and S. L. DeVore, "Interferogram evaluation and

wavefront fitting," in *Optical Shop Testing*, 2nd ed., D. Malacara, ed. (Wiley, New York, 1992), pp. 461–472.
6. G. D. Love, "Wave-front correction and production of Zernike modes with a liquid-crystal spatial light modulator," Appl. Opt. **36,** 1517–1524 (1997).
7. D. J. Cho, S. T. Thurman, J. T. Donner, and G. M. Morris, "Characteristics of a 128 × 128 liquid-crystal spatial light modulator for wave-front generation," Opt. Lett. **23,** 969–971 (1998).
8. F. Vargas-Martin and P. Artal, "Phasor averaging for wave-front correction with liquid-crystal spatial light modulators," Opt. Commun. **152,** 233–238 (1998).
9. M. A. A. Neil, M. J. Booth, and T. Wilson, "Dynamic wave-front generation for the characterization and testing of optical systems," Opt. Lett. **23,** 1849–1851 (1998).
10. G. Vdovin and P. M. Sarro, "Flexible mirror micromachined in silicon," Appl. Opt. **34,** 2968–2972 (1995).
11. L. Zhu, P.-C. Sun, D.-U. Bartsch, W. R. Freeman, and Y. Fainman, "Adaptive control of a micromachined continuous membrane deformable mirror for aberration compensation," Appl. Opt. **38,** 168–176 (1999).
12. L. Zhu, P.-C. Sun, and Y. Fainman, "Aberration-free dynamic focusing with a multichannel micromachined membrane deformable mirror," Appl. Opt. **38,** 5350–5354 (1999).